AIAA 78-1211R

# Supersonic Laminar Viscous Flow Past a Cone at Angle of Attack in Spinning and Coning Motion

Ramesh Agarwal* and John V. Rakich†
*NASA Ames Research Center, Moffett Field, Calif.*

**Computational results obtained with a parabolic Navier-Stokes marching code are presented for supersonic viscous flow past a pointed cone at angle of attack undergoing a combined spinning and coning motion. The code takes into account the asymmetries in the flowfield resulting from the motion and computes the asymmetric shock shape, crossflow and streamwise shear, heat transfer, crossflow separation and vortex structure. The side force and moment are also computed. Reasonably good agreement is obtained with the side force measurements of Schiff and Tobak. Comparison is also made with the only available numerical inviscid analysis. It is found that the asymmetric pressure loads due to coning motion are much larger than all other viscous forces due to spin and coning, making viscous forces negligible in the combined motion.**

## Nomenclature

c.g. = center of gravity
$c_p$ = specific heat at constant pressure divided by the freestream value
$C_m$ = normal moment (about c.g.) coefficient
$C_{m_\alpha} = \partial C_m/\partial\alpha$
$C_{m_{\dot\alpha}} = \partial C_m/\partial(\dot\alpha L/V_\infty)$
$C_{m_q} = \partial C_m/\partial(qL/V_\infty)$
$C_n$ = side moment (about c.g.) coefficient
$C_{n_{\dot\Phi}} = \partial C_n/\partial\dot\Phi$
$C_N$ = normal force coefficient
$C_{N_\alpha} = \partial C_N/\partial\alpha$
$C_{N_{\dot\alpha}} = \partial C_N/\partial(\dot\alpha L/V_\infty)$
$C_{N_q} = \partial C_N/\partial(qL/V_\infty)$
$C_Y$ = side force coefficient
$C_{Y_{\dot\Phi}} = \partial C_Y/\partial\dot\Phi$
$F_n$ = total normal force
$F_{p_w} = \frac{\sin 2\theta_c}{2}\int_0^x\int_0^{2\pi} x\sin\phi\, p_w(x,\phi)\,d\phi\,dx$
$F_s$ = total side force
$F_{\tau_x} = \sin^2\theta_c\int_0^x\int_0^{2\pi} x\sin\phi\,\tau_x(x,\phi)\,d\phi\,dx$
$F_{\tau_\phi} = \sin\theta_c\int_0^x\int_0^{2\pi} x\cos\phi\,\tau_\phi(x,\phi)\,d\phi\,dx$
$h$ = static enthalpy divided by freestream value
$\ell = \ell_c/L$
$\ell_c$ = distance of the center of gravity from the tip of the cone
$L$ = reference length
$M_\infty$ = freestream Mach number
$p$ = pressure divided by twice the freestream dynamic pressure
$Pr$ = freestream Prandtl number
$p_w$ = wall pressure
$q$ = pitch rate
$r$ = metric for the $\phi$ coordinate; $x\sin\theta + y\cos\theta$
$Re_\infty$ = freestream Reynolds number
$S$ = Sutherland's constant
$S_t$ = heat transfer coefficient
$T_0$ = freestream stagnation temperature in °R
$T_w$ = wall temperature in °R
$u$ = velocity in the $x$ direction divided by freestream velocity
$v$ = velocity in the $y$ direction divided by freestream velocity
$V_f$ = freestream velocity in rotating coordinate system
$V_\infty$ = freestream velocity
$w$ = velocity in the $\phi$ direction divided by freestream velocity
$x$ = coordinate along the rays of the cone surface divided by $L$
$y$ = coordinate normal to the surface divided by $L$
$\alpha$ = angle of attack
$\dot\alpha$ = time derivative of $\alpha$
$\gamma$ = ratio of specific heats
$\eta$ = transformed normal coordinate
$\theta_c$ = cone half angle
$\mu$ = viscosity divided by freestream viscosity
$\xi$ = bow-shock standoff distance divided by $L$
$\rho$ = density divided by freestream density
$\tau_x$ = primary flow wall shear stress
$\tau_\phi$ = crossflow wall shear stress
$\phi$ = circumferential coordinate
$\dot\Phi$ = coning rate parameter $= (2\pi/60)(\Omega_c L/V_\infty)$
$\Omega_s$ = spin angular velocity, rev/min
$\Omega_c$ = coning angular velocity, rev/min

Presented as Paper 78-1211 at the AIAA 11th Fluid and Plasma Dynamics Conference, Seattle, Wash., July 10-12, 1978; submitted Dec. 13, 1979; revision received Aug. 24, 1981. This paper is declared a work of the U.S. Government and therefore is in the public domain.

*NRC Research Associate. Presently Scientist at McDonnell Douglas Research Laboratories, St. Louis, Mo. Member AIAA.
†Research Scientist. Associate Fellow AIAA.

## I. Introduction

SUPERSONIC viscous flow past a projectile undergoing spinning and coning motion has been a problem of considerable interest in ballistics. Due to gyroscopic moments, a spinning projectile flying at an angle of attack undergoes a coning motion, wherein the nose of the body describes a circle around the flight velocity vector. At low angles of attack, coning motion has particular significance because the steady moment acting on a body of revolution in coning motion can be used to determine the damping-in-pitch derivatives that would be predicted by the linear theory of dynamic stability.

It appears that there have been only two previous theoretical investigations of the problem. Kuhn et al.[1] em-

ployed the potential theory and took into account empirically the presence of asymmetrically disposed leeside vortices at high angle of attack. Their theory had limited success in predicting the side force and moment at high angle of attack. Schiff,[2] on the other hand, used inviscid Euler equations in his numerical work. His inviscid analysis is adequate for calculating side force and moment due to coning motion at moderate angles of attack, so long as there is no crossflow separation on the leeside. However, it suffers from a number of drawbacks: 1) it cannot take into account the effect of spinning motion, 2) important physical quantities, such as primary flow and crossflow shear stresses, heat transfer rate, etc., cannot be calculated, 3) at high angles of attack, the vortex structure on the leeside cannot be computed.

In a previous work, Agarwal and Rakich[3] computed the flowfields of pointed and blunt spinning cones at high angle of attack by modifying the parabolic Navier-Stokes marching code due to Lubard and Helliwell.[4] In the present investigation, the same code is further modified to include the effect of coning motion. In the parabolic approximation, the viscous streamwise terms are assumed small (therefore neglected) compared with the viscous normal and circumferential derivatives in the steady-state Navier-Stokes and energy equations. The resulting equations are of the parabolic type which permit a marching solution from an initial data surface. The code treats the flow between the body surface and the bow shock wave by these parabolized equations which are valid both in the viscous and inviscid flow regions. No assumption or knowledge about the outer inviscid flowfield is required. The code takes into account the asymmetries in the flowfield resulting from spinning and coning motion and computes the asymmetric shock shape, crossflow and streamwise shear, heat transfer, crossflow separation, and vortex structure. The normal and side forces and moments are computed as well.

Modification of the code for the present application has required: 1) the inclusion of Coriolis and centrifugal force terms in the momentum equations (written in a rotating coordinate system), 2) the change in the shock boundary condition to account for the spatially varying rotating freestream, 3) the change in the body boundary condition to account for the spin, and 4) the deletion of the symmetry boundary condition in the circumferential direction.

The nature of the governing equations and the initial and boundary conditions are discussed, and the method for generating the starting solution is described. Results are presented for two sets of flow conditions. For one set, comparison is made with the experiment of Schiff and Tobak[5] and the inviscid calculation of Schiff.[2] For the other set, results are presented for a pointed cone in combined spinning and coning motion. The relative importance of viscous shear stresses and pressure forces in contributing to the side force in coning motion and Magnus force in spinning motion is ascertained.

## II. Formulation of the Problem

### Governing Equations

The governing equations are parabolized Navier-Stokes equations derived under the assumption that the gradients of the shear stress in the streamwise direction are negligibly small compared with the gradients in the normal and circumferential directions. In the development of these equations a *rotating* body-oriented coordinate system rotating with the angular velocity of the coning motion, fixed at the apex of the cone is used (Fig. 1), with $x$ taken along a cone generator, $y$ normal to the surface, and $\phi$ in the circumferential direction where $\phi=0$ represents the windward ray. The cone spins about its own axis and performs coning motion about an axis passing through its center of gravity (or some other point on the axis of the cone). The coordinate system *does not spin* with the body. The resulting nondimensional equations are as follows.

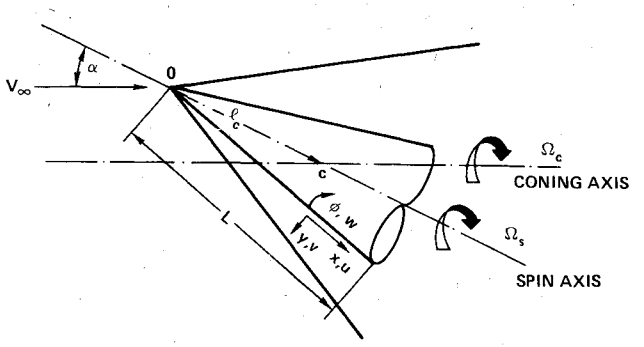


**Fig. 1 Pointed cone in spinning and coning motion (coordinate system).**

Continuity:

$$\frac{\partial(\rho ur)}{\partial x}+\frac{\partial(\rho vr)}{\partial y}+\frac{\partial(\rho w)}{\partial \phi}=0$$

$x$ momentum:

$$\frac{\partial(\rho u^2 r)}{\partial x}+\frac{\partial(\rho uvr)}{\partial y}+\frac{\partial(\rho wu)}{\partial \phi}-\rho w^2\sin\theta_c+r\frac{\partial p}{\partial x}$$
$$+\rho r[2(\Omega_y w-\Omega_\phi v)-(\Omega_\phi^2+\Omega_y^2)(x-\ell\cos\theta_c)$$
$$+\Omega_x\Omega_y(y+\ell\sin\theta_c)]=\frac{r}{Re_\infty}\left[\frac{\partial}{\partial y}\left(\mu\frac{\partial u}{\partial y}\right)+\frac{1}{r^2}\frac{\partial}{\partial \phi}\left(\mu\frac{\partial u}{\partial \phi}\right)\right]$$

$y$ momentum:

$$\frac{\partial(\rho uvr)}{\partial x}+\frac{\partial(\rho v^2 r)}{\partial y}+\frac{\partial(\rho wv)}{\partial \phi}-\rho w^2\cos\theta_c+r\frac{\partial p}{\partial y}$$
$$+\rho r[2(\Omega_\phi u-\Omega_x w)-(\Omega_\phi^2+\Omega_x^2)(y+\ell\sin\theta_c)$$
$$+\Omega_x\Omega_y(x-\ell\cos\theta_c)]=\frac{r}{Re_\infty}\left[\frac{4}{3}\frac{\partial}{\partial y}\left(\mu\frac{\partial v}{\partial y}\right)\right.$$
$$\left.+\frac{1}{r^2}\frac{\partial}{\partial \phi}\left(\mu\frac{\partial v}{\partial \phi}\right)-\frac{2}{3r}\frac{\partial}{\partial y}\left(\mu\frac{\partial w}{\partial \phi}\right)+\frac{1}{r}\frac{\partial}{\partial \phi}\left(\mu\frac{\partial w}{\partial y}\right)\right]$$

$\phi$ momentum:

$$\frac{\partial(\rho uwr)}{\partial x}+\frac{\partial(\rho vwr)}{\partial y}+\frac{\partial(\rho w^2)}{\partial \phi}+\rho uw\sin\theta_c+\rho wv\cos\theta_c$$
$$+\frac{\partial p}{\partial \phi}+\rho r[2(\Omega_x v-\Omega_y u)+\Omega_y\Omega_\phi(y+\ell\sin\theta_c)$$
$$+\Omega_x\Omega_\phi(x-\ell\cos\theta_c)]=\frac{r}{Re_\infty}\left[\frac{\partial}{\partial y}\left(\mu\frac{\partial w}{\partial y}\right)+\frac{4}{3r^2}\frac{\partial}{\partial \phi}\left(\mu\frac{\partial w}{\partial \phi}\right)\right.$$
$$\left.+\frac{1}{r}\frac{\partial}{\partial y}\left(\mu\frac{\partial v}{\partial \phi}\right)-\frac{2}{3r}\frac{\partial}{\partial \phi}\left(\mu\frac{\partial v}{\partial y}\right)\right]$$

Energy:

$$\frac{\partial(\rho uhr)}{\partial x}+\frac{\partial(\rho vhr)}{\partial y}+\frac{\partial(\rho wh)}{\partial \phi}-r(\gamma-1)M_\infty^2\left(u\frac{\partial p}{\partial x}+v\frac{\partial p}{\partial y}\right.$$
$$\left.+\frac{w}{r}\frac{\partial p}{\partial \phi}\right)=\frac{r}{Re_\infty Pr}\left[\frac{\partial}{\partial y}\left(\frac{k}{c_p}\frac{\partial h}{\partial y}\right)+\frac{1}{r^2}\frac{\partial}{\partial \phi}\left(\frac{k}{c_p}\frac{\partial h}{\partial \phi}\right)\right]$$
$$+\frac{(\gamma-1)M_\infty^2 r}{Re_\infty}\left[\mu\left(\frac{\partial u}{\partial y}\right)^2+\frac{\mu}{r^2}\left(\frac{\partial u}{\partial \phi}\right)^2+\frac{4\mu}{3}\left(\frac{\partial v}{\partial y}\right)^2\right.$$

$$+\frac{\mu}{r^2}\left(\frac{\partial v}{\partial\phi}\right)^2+\mu\left(\frac{\partial w}{\partial y}\right)^2+\frac{4\mu}{3r^2}\left(\frac{\partial w}{\partial\phi}\right)^2-\frac{4\mu}{3r}\frac{\partial v}{\partial y}\frac{\partial w}{\partial\phi}$$

$$+\frac{2\mu}{r}\frac{\partial v}{\partial\phi}\frac{\partial w}{\partial y}\Bigg]$$

Equation of state (perfect gas):

$$\rho=\gamma M_\infty^2\,(p/h)$$

Viscosity law (Sutherland's):

$$\mu=\frac{\sqrt{h}(1+S)}{1+S/h}$$

Here $(\Omega_x, \Omega_y, \Omega_\phi)$ are angular velocity components of the coning motion, given as:

$$\Omega_x=\dot\Phi(-\cos\theta_c\cos\alpha+\sin\theta_c\sin\alpha\cos\phi)$$

$$\Omega_y=\dot\Phi(\sin\theta_c\cos\alpha+\cos\theta_c\sin\alpha\cos\phi)$$

$$\Omega_\phi=-\dot\Phi\sin\alpha\sin\phi$$

where

$$\dot\Phi=\text{coning rate}=\frac{2\pi}{60}\frac{\Omega_c L}{V_\infty}$$

Prandtl number and specific heat are assumed constant.

#### Boundary Conditions

The following boundary conditions at the cone surface are used:

$$u=v=0;\quad w=w_w=\frac{2\pi}{60}\frac{\Omega_s L}{V_\infty}x\sin\theta_c$$

$$h_w=c_p T_w=\text{specified constant}$$

$$\left(\frac{\partial p}{\partial y}\right)_w=\frac{1}{Re_\infty}\left(\frac{4\mu}{3}\frac{\partial^2 v}{\partial y^2}+\frac{\mu}{3r}\frac{\partial^2 w}{\partial y\partial\phi}\right)+\frac{\rho w^2\cos\theta_c}{r}$$

$$+\rho[2\Omega_x w+(\Omega_\phi^2+\Omega_x^2)\ell\sin\theta_c-\Omega_x\Omega_y(x-\ell\cos\theta_c)]$$

To obtain the outer boundary conditions, Rankine-Hugoniot conditions are utilized at the shocks.

The density, static pressure, and static enthalpy in the freestream remain constant with respect to the body-fixed rotating coordinate system. However, the components of freestream velocity vary and are given as:

$$u_f(x,\phi)=\cos\theta_c\cos\alpha-\sin\theta_c\sin\alpha\cos\phi+\Omega_\phi(\xi+\ell\sin\theta_c)$$

$$v_f(x,\phi)=-\sin\theta_c\cos\alpha-\cos\theta_c\sin\alpha\cos\phi-\Omega_\phi(x-\ell\cos\theta_c)$$

$$w_f(x,\phi)=\sin\phi\sin\alpha-\Omega_x(\xi+\ell\sin\theta_c)+\Omega_y(x-\ell\cos\theta_c)$$

where $\xi=\xi(x,\phi)$.

The Rankine-Hugoniot jump conditions then can be written as follows.

Conservation of mass:

$$(u_f-\rho_k u_k)\frac{\partial\xi}{\partial x}-(v_f-\rho_k v_k)+(w_f-\rho_k w_k)\frac{1}{r}\frac{\partial\xi}{\partial\phi}=0$$

Conservation of normal momentum:

$$\frac{\left(u_f\frac{\partial\xi}{\partial x}-v_f+\frac{w_f}{r}\frac{\partial\xi}{\partial\phi}\right)^2}{\left(\frac{\partial\xi}{\partial x}\right)^2+1+\left(\frac{1}{r}\frac{\partial\xi}{\partial\phi}\right)^2}+p_f=\frac{\left(u_k\frac{\partial\xi}{\partial x}-v_k+\frac{w_k}{r}\frac{\partial\xi}{\partial\phi}\right)^2}{\left(\frac{\partial\xi}{\partial x}\right)^2+1+\left(\frac{1}{r}\frac{\partial\xi}{\partial\phi}\right)^2}+p_k$$

Conservation of tangential momentum:

$$(u_f-u_k)\left[\frac{1}{r^2}\left(\frac{\partial\xi}{\partial\phi}\right)^2+1\right]+(v_f-v_k)\frac{\partial\xi}{\partial x}$$

$$-\frac{(w_f-w_k)}{r}\frac{\partial\xi}{\partial\phi}\frac{\partial\xi}{\partial x}=0$$

$$(v_f-v_k)\frac{1}{r}\frac{\partial\xi}{\partial\phi}+(w_f-w_k)=0$$

Conservation of energy:

$$1+\frac{(\gamma-1)}{2}M_\infty^2 V_f^2=h_k+\frac{(\gamma-1)}{2}M_\infty^2(u_k^2+v_k^2+w_k^2)$$

The subscript $k$ denotes the value of the variable just inside the shock. To uniquely determine the six unknowns $\xi$, $u_k$, $v_k$, $w_k$, $p_k$, $h_k$, the above five equations must be augmented with another equation which matches the shock to the state of the downstream flow. A one-sided differencing of the continuity equation provides the sixth equation.

Since the windward and leeward surfaces are not symmetry planes for the cone in spinning and coning motion, a periodicity condition for the flow profiles in the windward plane is specified.

In a rectangular $y-\phi$ grid, the shock may not fall on a mesh point, so that the mesh points would have to be moved or added to accommodate the shock. Thus, the transformation $\eta=y/\xi(x,\phi)$ is made. The resulting equations are then solved for $0\le\eta\le1$, $0\le\phi\le2\pi$, where $\eta=0$ corresponds to the cone and $\eta=1$ corresponds to the shock. The shock distance $\xi$ appears in all the equations. To keep the matrix of coefficients obtained from the difference form of the equations in the block tridiagonal form, a sixth equation, $\partial\xi/\partial\eta=0$, is differenced. Thus, the problem to be solved consists of six differential equations, six boundary conditions at each of the positions $\eta=0$ and $\eta=1$, and a periodicity condition for the flow profiles at $\phi=0$ or $2\pi$. With the specification of initial conditions, a marching scheme in $x$ can be used to solve the equations.

## III. Method of Solution

#### Numerical Scheme

Details of the numerical differencing scheme, together with analysis of convergence and stability criteria, are given by Lubard and Helliwell.[4] The differencing scheme used can be termed as implicit-iterative. The normal derivatives are differenced completely implicitly, that is, at the new $x$ station and new iterate. The circumferential derivatives are differenced at the new $x$ station while only the central and backward term is taken at the new iterate. Newton's method of iteration is then used to solve the nonlinear algebraic equations which result from the differencing. It is known that this iteration procedure converges if the initial guess is close enough to the solution, and linearly extrapolating the solution at the previous two $x$ stations seems to give a satisfactory initial guess. This numerical scheme of Lubard and Helliwell[4] imposes lower as well as upper bound restrictions on the step size $\Delta x$ in the marching direction: there is an upper bound restriction on $\Delta x$ for convergence and a lower bound restriction to avoid departure solutions. A careful selection of $\Delta x$, $\Delta y$, and $\Delta\phi$ is necessary to obtain a solution.

**Generation of Initial Conditions**

The code requires as input the flow profiles and shock standoff distance at some initial station. For a sharp cone an approximate starting solution is obtained by constructing a suitable analytical shock shape from the shock angles due to the flow past a locally tangent wedge. The inviscid flowfield between the cone and the bow shock is obtained by using Rankine-Hugoniot jump relations across the bow shock. Then an approximate Blasius type boundary-layer solution is constructed between the body and the bow shock, taking into account the spin on the body. Experience has shown that a fairly good starting solution is thus obtained, even at very high angles of attack.

## IV. Results and Discussion

The results are presented in two parts for two sets of flow conditions. In part A, the flow conditions are those of the experiment by Schiff and Tobak[5] and used by Schiff[2] in his inviscid computations. The cone is undergoing only the coning motion about the center of gravity. Comparisons are made with the inviscid solution of Schiff[2] and the force and moment measurements of Schiff and Tobak.[5] In part B, the flow conditions are those used by Sanders and Dwyer[6] as well as Agarwal and Rakich[3] in their computations of the flowfield of a spinning cone. For this set of flow conditions, the cone performs the combined spinning and coning motion. Comparisons of the magnitudes of the side force and moment in the combined motion are made with the Magnus force and moment (due to spin alone) to ascertain the relative importance of viscous shear stresses and pressure forces for the Magnus problem and the coning problem.

### A. Flow Conditions: Coning Motion

$$M_\infty = 2, \quad Re_\infty = 2.79 \times 10^6, \quad Pr = 0.72, \quad T_w/T_0 = 0.9527$$

$$L = 56.74218 \text{ cm } (1.86162 \text{ ft}), \quad \ell = 0.60073, \quad \Omega_c = 1077 \text{ rpm}$$

$$\theta_c = 10 \text{ deg}, \quad \alpha = (2.5, 5, \text{and } 7.5 \text{ deg})$$

Figures 2 and 3 show the variation of the normal force and moment coefficients, and the side force and moment coefficients, respectively, with angle of attack. Agreement with the experimental measurements of Schiff and Tobak[5] is reasonably good, and with the inviscid computations of Schiff,[2] it is excellent. For the range of the angles of attack considered, the normal force and moment coefficients due to coning are also in good agreement with the predictions of the perturbation theory (Ref. 7). Side force and moment derivatives due to coning $C_{y_\dot{\Phi}}$ and $C_{n_\dot{\Phi}}$ agree well with the damping in pitch derivatives $\alpha(C_{N_q} + C_{N_\dot{\alpha}})$ and $\alpha(C_{m_q} + C_{m_\dot{\alpha}})$, respectively, predicted by the perturbation theory of Brong.[8] The equivalence of $C_{y_\dot{\Phi}}$ and $C_{n_\dot{\Phi}}$ with $\alpha(C_{N_q} + C_{N_\dot{\alpha}})$ and $\alpha(C_{m_q} + C_{m_\dot{\alpha}})$, respectively, is discussed in Ref. 2. In Table 1, the numerical values of normal, side force, and moment coefficients are compared with the inviscid computations of Schiff[2] to demonstrate once again the excellent agreement of inviscid and viscous computations. This suggests that the viscous forces do not significantly affect the aerodynamic coefficients and this, indeed, is borne out in the present computations.

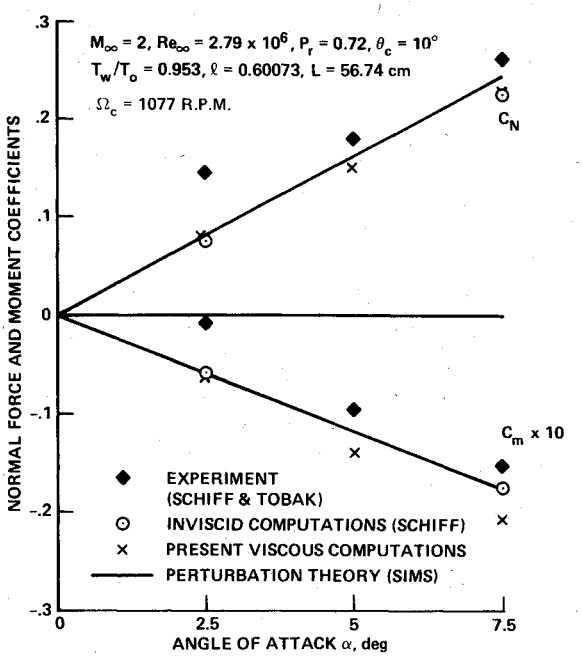


Fig. 2 Variation of normal force ($C_N$) and moment ($C_m$) coefficients with angle of attack for a cone in coning motion.

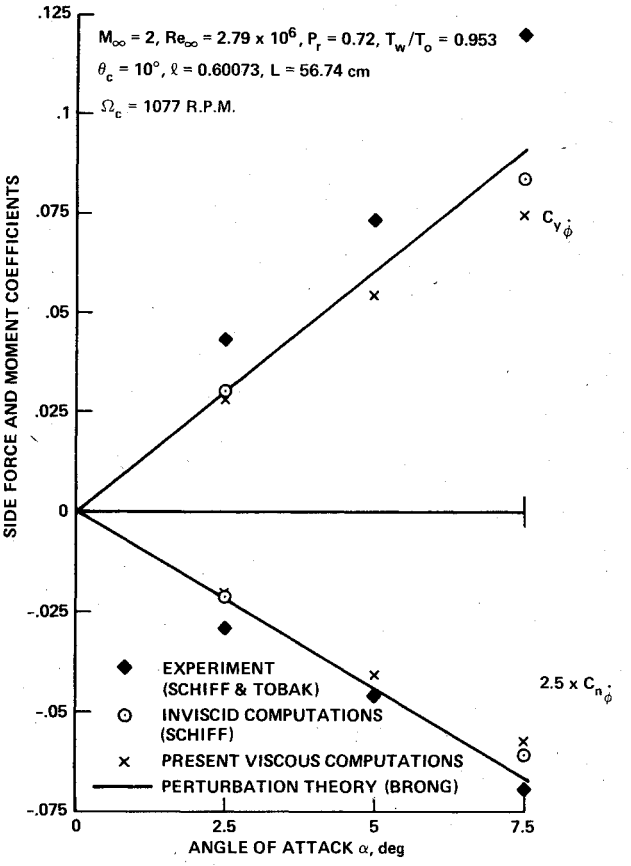


Fig. 3 Variation of side force ($C_{y_\dot{\Phi}}$) and moment ($C_{n_\dot{\Phi}}$) coefficients with angle of attack for a cone in coning motion.

Table 1 Comparison of normal and side force and moment coefficients from inviscid and viscous computations

| | $C_N$ | | $C_m$ | | $C_{y_\dot{\Phi}}$ | | $C_{n_\dot{\Phi}}$ | |
|---|---|---|---|---|---|---|---|---|
| $\alpha$, deg | Schiff[2] | Present | Schiff[2] | Present | Schiff[2] | Present | Schiff[2] | Present |
| 2.5 | 0.07562 | 0.07896 | −0.005864 | −0.006403 | 0.029744 | 0.02861 | −0.008303 | −0.00838 |
| 5 | ... | 0.15095 | ... | −0.014035 | ... | 0.05417 | ... | −0.01620 |
| 7.5 | 0.22640 | 0.22907 | −0.017553 | −0.020734 | 0.08386 | 0.07394 | −0.024715 | −0.02361 |

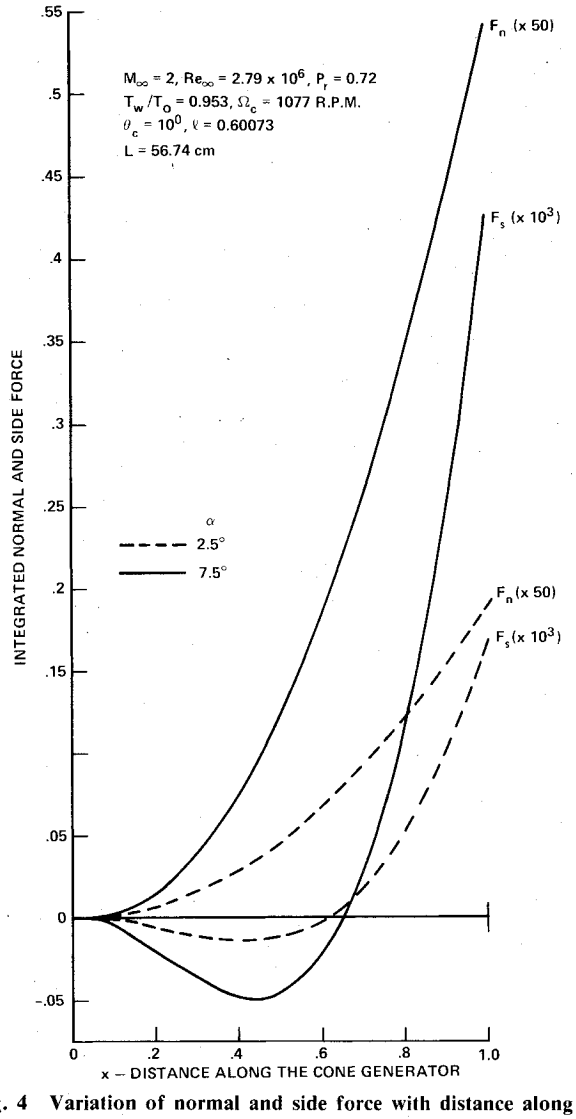


**Fig. 4 Variation of normal and side force with distance along the cone-generator for a cone in coning motion.**

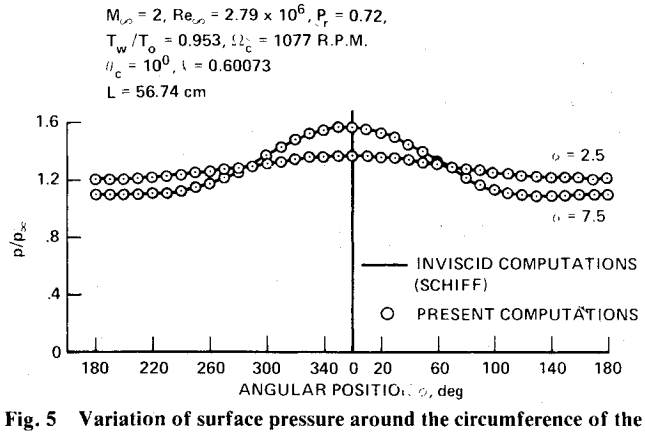


**Fig. 5 Variation of surface pressure around the circumference of the cone in coning motion at $x = 1$.**

In Fig. 4, the variation of the normal and side force along the cone generator is shown for two angles of attack. It is interesting to note that the integrated side force changes sign close to the center of gravity because of the coning motion. Normal force, however, varies monotonically with distance along the cone generator. Normal forces are two orders-of-magnitude higher than the side forces.

In Fig. 5, pressure around the circumference of the cone is compared with the inviscid results of Schiff[2] at two angles of

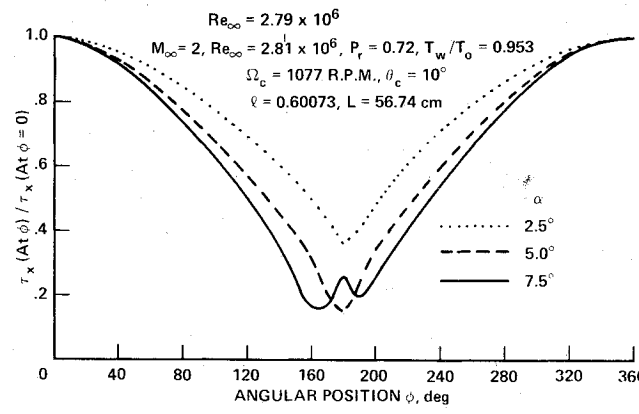


**Fig. 6 Variation of primary flow wall shear relative to windside around the circumference of a cone in coning motion at $x = 1$.**

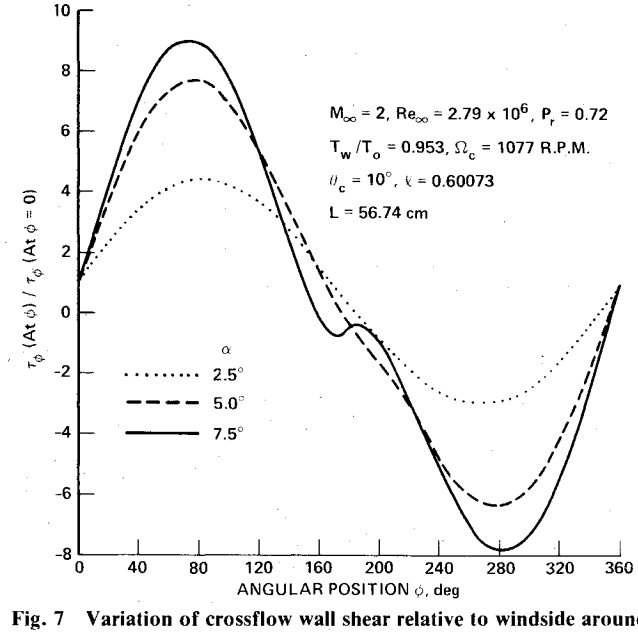


**Fig. 7 Variation of crossflow wall shear relative to windside around the circumference of a cone in coning motion at $x = 1$.**

attack and again the agreement is excellent. Figures 6, 7, and 8 show the variation of streamwise shear, crossflow shear, and Stanton number, respectively, relative to the windside around the circumference of the cone at various angles of attack. In Figs. 9 and 10, crossflow velocity profiles in the shock layer are plotted at various circumferential locations around the cone.

### B. Flow Conditions: Combined Spinning and Coning Motion

$$M_\infty = 4, \quad Re_\infty = (2.81 \times 10^5 \text{ and } 2.81 \times 10^6)$$

$$Pr = 1, \quad T_w/T_0 = 0.24, \quad L = 30.48 \text{ cm (1 ft)}, \quad \ell = 0.61$$

$$\theta_c = 10 \text{ deg}, \quad \alpha = (2, 4, 6, \text{and } 10 \text{ deg})$$

$$\Omega_c = 4468 \text{ rpm}, \quad \Omega_s = 30{,}000 \text{ rpm}$$

Figure 11 shows the variation of the normal force and moment coefficient with angle of attack for a stationary cone, a spinning cone, and a cone in combined spinning and coning motion. Coning or spinning motion has little effect on normal force and moment. Figure 12 shows the variation of the side force and moment coefficient with angle of attack for a cone in the combined spinning and coning motion. In Fig. 13, the variation in the side force (a result of asymmetric pressure distribution around the circumference of the cone) along the cone generator due to combined spinning and coning motion

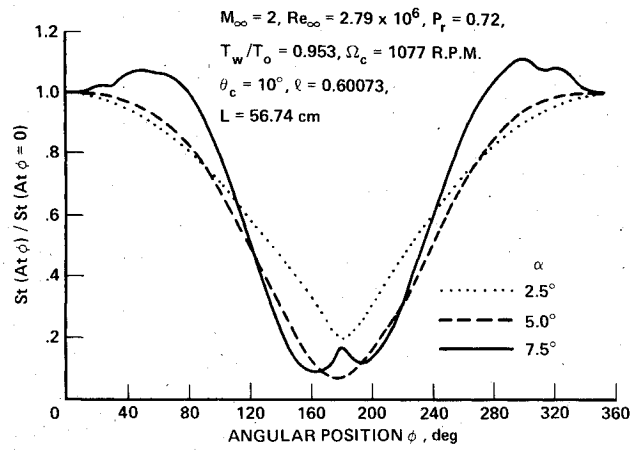


**Fig. 8 Variation of heat-transfer coefficient relative to windside around the circumference of a cone in coning motion at $x = 1$.**

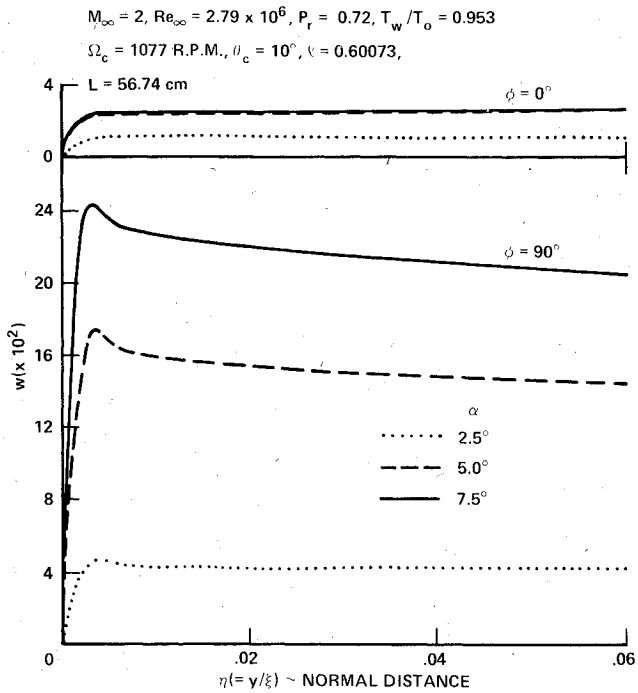


**Fig. 9 Crossflow velocity profiles in the shock layer at $x = 1$ for a cone in coning motion.**

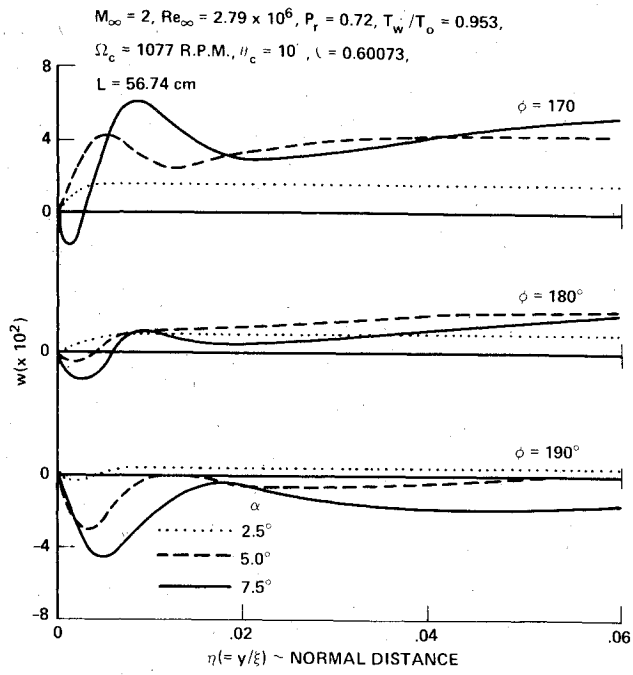


**Fig. 10 Crossflow velocity profiles in the shock layer at $x = 1$ for a cone in coning motion.**

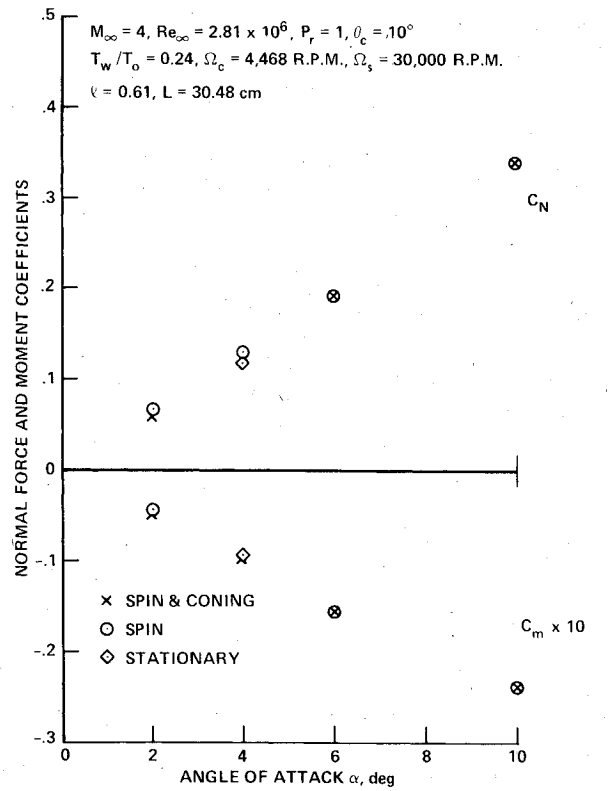


**Fig. 11 Variation of normal force ($C_N$) and moment ($C_m$) coefficients with angle of attack for a cone in spinning and coning motion.**

is shown for a cone at 4 deg angle of attack at two Reynolds numbers and is compared with the variation in the Magnus force with $x$ at the corresponding Reynolds numbers. In the combined motion, the change in the Reynolds number does not significantly affect the magnitude of the side force. Magnus force, however, changes depending on the Reynolds number.[3] Since the Magnus force is nearly an order-of-magnitude smaller than the side force due to coning, the Magnus contribution to the combined motion becomes relatively small. Thus in the combined motion at moderate coning rates, the effect of spinning on the aerodynamic coefficients can be considered negligible.

Figure 14 shows the variation in side force (due to shear stresses $\tau_x$ and $\tau_\phi$) along the cone generator at two Reynolds numbers in the combined motion and its comparison with the corresponding Magnus components. It is clear that the shear stresses in the combined motion are not significantly different from those in the spinning motion alone. Considering the magnitude of the contribution to side force due to $\tau_x$ and $\tau_\phi$ as compared to that due to $p_w$, it is clear that in the combined motion, the contribution to side force due to $\tau_x$ and $\tau_\phi$ is relatively small compared to that due to $p_w$. In spinning motion, however, the contribution to Magnus force due to $\tau_\phi$ is of the same order-of-magnitude as that of $p_w$.

In Fig. 15 the variation of heat-transfer coefficient, relative to the windside value around the circumference, is plotted for a stationary cone, a cone in spinning motion, and in combined spinning and coning motion. Again, coning does not change the laminar heat-transfer characteristics significantly.

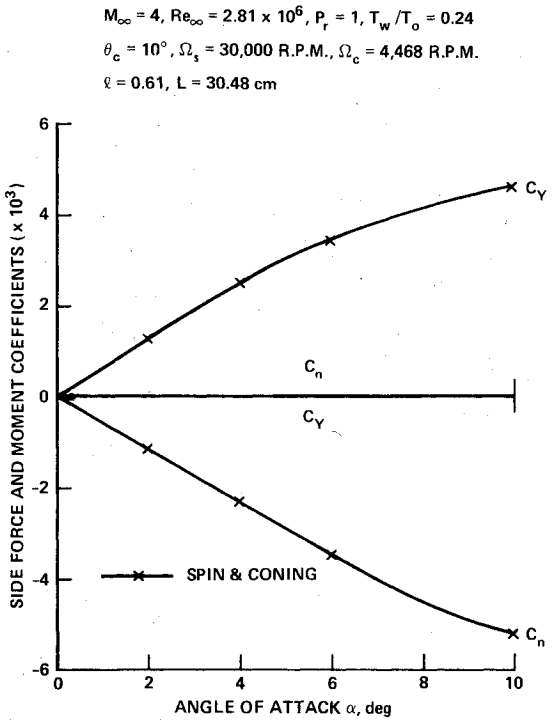


**Fig. 12 Variation of side force ($C_Y$) and moment ($C_n$) coefficients with angle of attack for a cone in spinning and coning motion.**

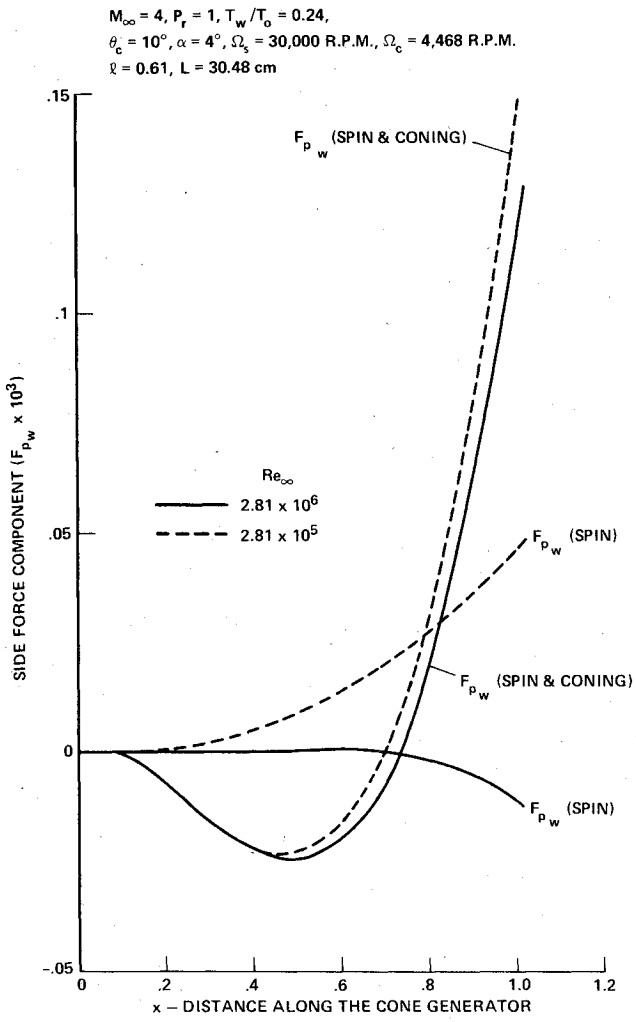


**Fig. 13 Variation of side force component $F_{pw}$ with distance along the cone generator for a cone in coning and spinning motion.**

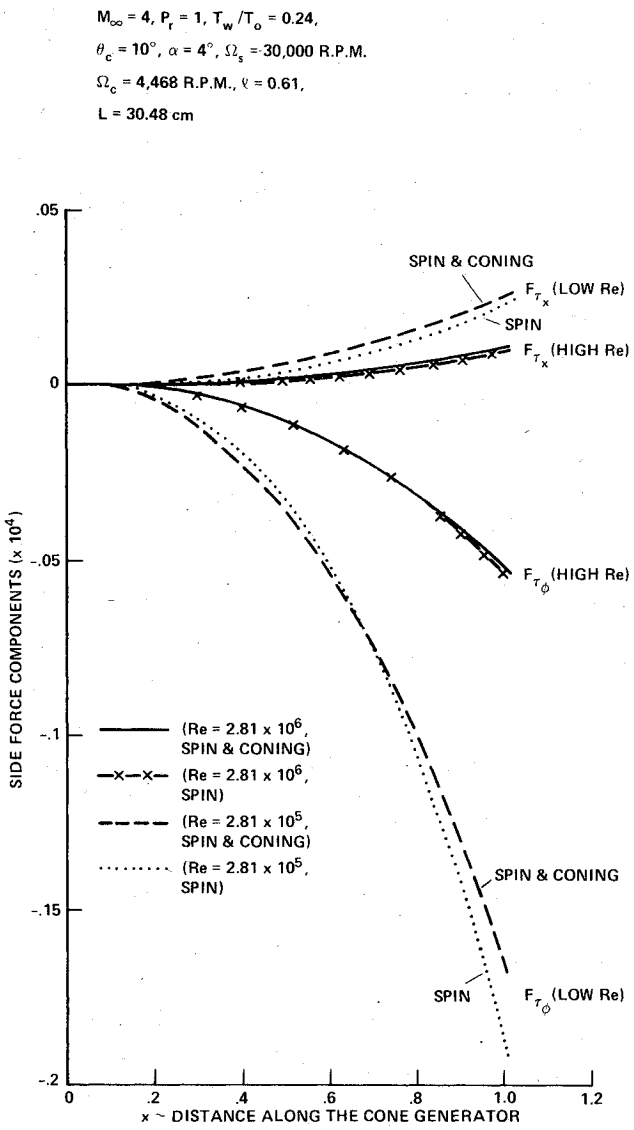


**Fig. 14 Variation of side force components $F_{\tau x}$ and $F_{\tau\phi}$ with distance along the cone generator for a cone in spinning and coning motion.**

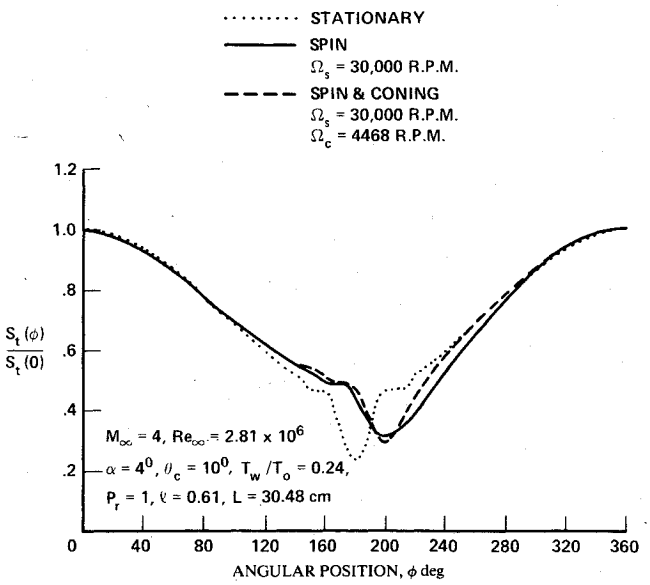


**Fig. 15 Variation of heat-transfer coefficient relative to windside around the circumference of a cone in spinning and coning motion at $x = 0.8$.**

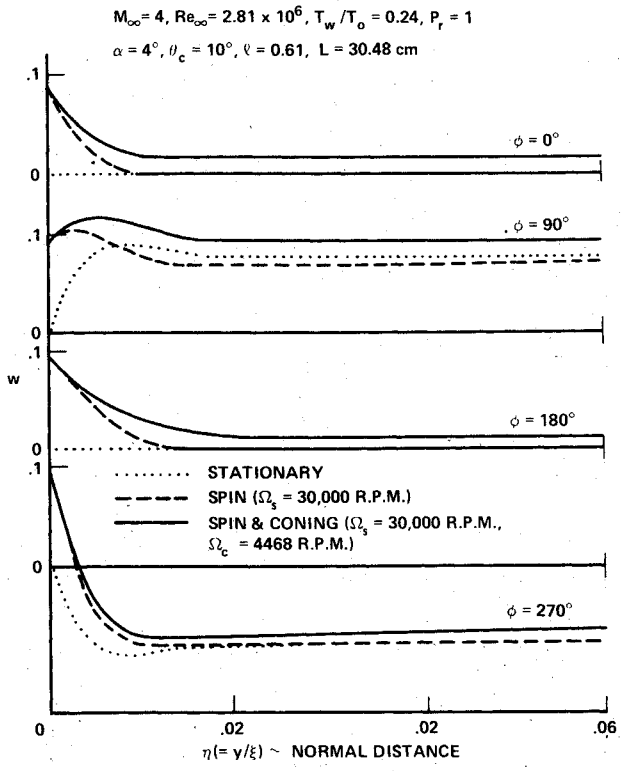


**Fig. 16 Crossflow velocity profiles in the shock layer at $x = 0.8$ for a cone in spinning and coning motion.**

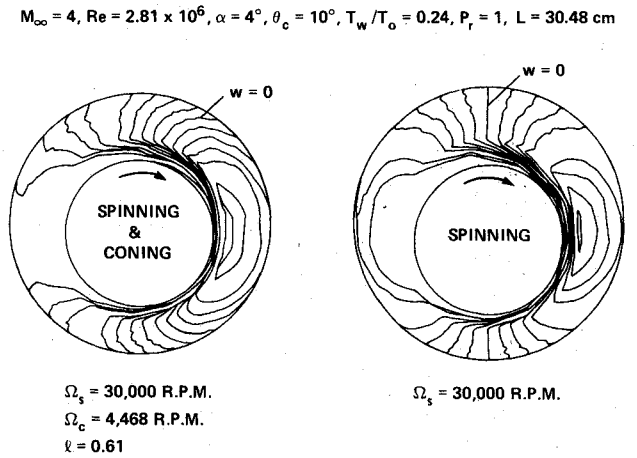


**Fig. 17 Crossflow velocity contours at $x = 0.8$ (location past c.g.) for a cone in spinning and coning motion. Coning direction ⊙.**

In Fig. 16, a comparison of the crossflow velocity profiles at various circumferential locations around the cone is presented for a stationary cone, a spinning cone, and a cone in combined spinning and coning motion. Finally, in Fig. 17, crossflow velocity contours are shown for a cone in spinning and in combined spinning and coning motion. Coning further accentuates the asymmetry in the flowfield.

## V. Summary

For the first time, the viscous flowfield of a pointed cone undergoing spinning as well as coning motion at an angle of attack has been calculated using the parabolized Navier-Stokes and energy equation approximation. The main result of the present work can be summarized as follows:

1) While the viscous shear stresses as well as the pressure forces are important in the computation of Magnus force and moment, as has been pointed out in Agarwal and Rakich,[3] only the pressure forces are important in the computation of side force due to coning motion, at the angles of attack, coning and spinning rates considered in this paper. The contribution to side force due to asymmetry in the inviscid pressure resulting from coning motion is so large that the contribution due to all other viscous forces can be assumed negligible.

2) Coning or spinning motion has negligibly small effect on normal force and moment.

3) At small angles of attack, the side force and moment derivatives ($C_{y\dot{\Phi}}$ and $C_{n\dot{\Phi}}$) due to coning in the present computations are in good agreement with the perturbation theory of Brong.[8] At high angles of attack, nonlinear effects become important.

## References

[1] Kuhn, G. D., Spangler, S. B., and Nielsen, J. N., "Theoretical Analysis of Vortex Shedding from Bodies of Revolution in Coning Motion," *AIAA Journal*, Vol. 9, June 1971, pp. 784-790.

[2] Schiff, L. B., "A Study of the Nonlinear Aerodynamics of Bodies in Nonplanar Motion," NASA TR 4-421, Jan. 1974.

[3] Agarwal, R. and Rakich, J. V., "Computation of Hypersonic Laminar Viscous Flow Past Spinning Sharp and Blunt Cones at High Angle of Attack," AIAA Paper 78-65, Jan. 1978.

[4] Lubard, S. C. and Helliwell, W. S., "Calculation of the Flow on a Cone at High Angle of Attack," R&D Associates, Santa Monica, Calif., RDA TR 150, Feb. 1973.

[5] Schiff, L. B. and Tobak, M., "Results from a New Wind-Tunnel Apparatus for Studying Coning and Spinning Motions of Bodies of Revolution," *AIAA Journal*, Vol. 8, Nov. 1970, pp. 1953-1957.

[6] Sanders, B. R. and Dwyer, H. A., "Magnus Forces on Spinning Supersonic Cones—Part II: Inviscid Flow," *AIAA Journal*, Vol. 14, May 1976, pp. 576-582.

[7] Sims, J. L., "Supersonic Flow Around Right Circular Cone Tables for Small Angles of Attack," Rept. No. DA-TR-19-60, April 1960.

[8] Brong, E. A., "The Unsteady Flow Field About a Right Circular Cone in Unsteady Flight," AFFDL-TDR-64-148, Jan. 1967.